Advancing H&E-to-IHC Virtual Staining with Task-Specific Domain Knowledge for HER2 Scoring

Qiong Peng[1], Weiping Lin[1], Yihuang Hu[1], Ailisi Bao[2], Chenyu Lian[1], Weiwei Wei[3], Meng Yue[4], Jingxin Liu[5], Lequan Yu[6], and Liansheng Wang[1] (✉)

[1] Department of Computer Science at School of Informatics, Xiamen University, Xiamen, China
{qpeng, wplin, huyihuang, cylian}@stu.xmu.edu.cn, lswang@xmu.edu.cn
[2] School of Information, Central University of Finance and Economics, Beijing, China
ailisilob@163.com
[3] Medicine AI Lab, Clinvita-Intelligent Pathology Center, Shanghai, China
wei01@clinvita.vip
[4] Department of Pathology, The Fourth Hospital of Hebei Medical University, Hebei, China
mengyue0831@163.com
[5] School of AI and Advanced Computing, Xi'an Jiaotong-Liverpool University, Suzhou, China
jingxin.liu@xjtlu.edu.cn
[6] Department of Statistics and Actuarial Science, The University of Hong Kong, Pok Fu Lam, Hong Kong SAR, China
lqyu@hku.hk

Abstract. The assessment of HER2 expression is crucial in diagnosing breast cancer. Staining pathological tissues with immunohistochemistry (IHC) is a critically pivotal step in the assessment procedure, while it is expensive and time-consuming. Recently, generative models have emerged as a novel paradigm for virtual staining from hematoxylin-eosin (H&E) to IHC. Unlike traditional image translation tasks, virtual staining in IHC for HER2 scoring requires greater attention to regions like nuclei and stained membranes, informed by task-specific domain knowledge. Unfortunately, most existing virtual staining methods overlook this point. In this paper, we propose a novel generative adversarial network (GAN) based solution that incorporates specific knowledge of HER2 scoring, i.e., nuclei distribution and membrane staining intensity. We introduce a nuclei density estimator to learn the nuclei distribution and thus facilitate the cell alignment between the real and generated images by an auxiliary regularization branch. Moreover, another branch is tailored to focus on the stained membranes, ensuring a more consistent membrane staining intensity. We collect RegH2I, a dataset comprising 2592 pairs of registered H&E-IHC images and conduct extensive experiments to evaluate our approach, including H&E-to-IHC virtual

Q. Peng and W. Lin——Contributed equally.

staining on internal and external datasets, nuclei distribution and membrane staining intensity analysis, as well as downstream tasks for generated images. The results demonstrate that our method achieves superior performance than existing methods. Code and dataset are released at https://github.com/balball/TDKstain.

Keywords: H&E-to-IHC virtual staining · Generative adversarial network · Domain knowledge · HER2 scoring.

1 Introduction

The function of Human Epidermal Growth Factor Receptor 2 (HER2) is to regulate cell growth and division. In certain cancers, the overexpression of HER2 can result in excessive tumor growth and malignant transformation [4, 8, 21]. Thus, HER2 is referred to as a cancer biomarker. Accurate assessments of HER2 expression require immunohistochemical (IHC) staining for pathological tissues, which entails expensive antibodies and intricate experimental procedures [6, 12].

With recent advancements in digital pathology and deep learning, generative models have emerged as a novel paradigm for virtual staining [2, 18]. Liu *et al.* [13] proposed a variant of Pix2pix [9] called Pyramidpix2pix, which employed Gaussian convolutions on image pairs at multiple scales to weaken the constraints of pixel-level alignment for H&E-to-IHC stain translation. Besides, Li *et al.* [11] presented a novel loss function to deal with the input-to-target inconsistencies by mitigating the negative impact of noisy supervision. Furthermore, some methods have incorporated prior pathological knowledge from experts into their networks, such as segmentation annotations [14] and patch-level labels [23], to preserve representative pathology phenotypes. Leveraging well-trained generative models, complex IHC-stained images can be directly generated from readily available H&E-stained images, significantly simplifying the process and reducing costs.

Different stained images from consecutive cuts exhibit inherent differences even before staining, thus resulting in a lack of nearly perfect pixel-level registration between image pairs. Additionally, cellular and tissue structures exhibit strong homogeneity, resulting in minimal visual distinctions between images containing different diagnostic information. Thus, unlike traditional image translation tasks that usually seek perfect pixel alignment, virtual staining focuses more on specific regions, which are determined by medical knowledge. According to the guidelines [1], HER2 scoring primarily focuses on the quantity of infiltrating carcinoma cells and the intensity of membrane staining. Thus, the nuclei distribution and membrane staining should be exactly accurate in the generated images. However, most existing virtual staining methods for HER2 scoring do not comprehensively consider the task-specific knowledge. In this case, even though the visual difference between the real and generated images is minimal, critical information essential for clinical diagnosis might still be lost.

To address this gap, in this paper, we propose a novel Generative Adversarial Network (GAN) based solution that incorporates specific medical knowledge of

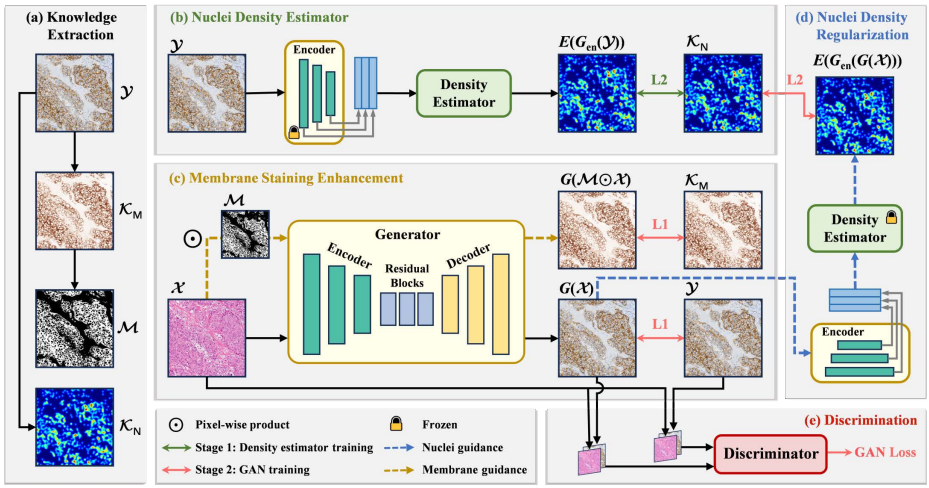

Fig. 1. Overview of the proposed framework. (a) Knowledge extraction to obtain nuclei density map, membrane staining channel and its intensity mask. (b) A nuclei density estimator deployed to depict the nuclei distribution. (c) An auxiliary branch to guide GAN focusing on membrane staining regions. (d) An auxiliary branch to promote nuclei distribution alignment. (e) A discriminator in GAN training. Note that the encoder and nuclei density estimator in different modules share weights.

HER2 scoring, particularly the nuclei distribution and membrane staining intensity. We conduct extensive experiments to evaluate our approach, including H&E-to-IHC virtual staining on internal and external datasets, nuclei distribution and membrane staining analysis, as well as downstream tasks for generated images. And our proposed method consistently outperforms existing methods. Overall, our primary contributions can be summarized as follows: (1) We collect and build RegH2I: a well-registered H&E to IHC image translation dataset for HER2 scoring. (2) We propose a novel GAN for H&E-to-IHC virtual staining in HER2 scoring, guided by specific domain knowledge, enriching diagnosis information in the generated images. (3) We introduce a nuclei density estimator to learn the nuclei distribution, promoting the cell alignment between the real and generated images by an auxiliary regularization branch. (4) We tailor another auxiliary branch to guide the model focus on the membrane staining regions, ensuring a more consistent membrane staining intensity.

2 Method

Fig. 1 illustrates the overview of our method. Given real H&E-stained images $\{x_i\}_{i=1}^{N} \in \mathcal{X}$ and real IHC-stained images $\{y_i\}_{i=1}^{N} \in \mathcal{Y}$, our objective is to train a generator G to minimize the inconsistency between $G(\mathcal{X})$ and $\mathcal{Y}$. Initially, we extract task-specific domain knowledge in HER2 scoring, as depicted in Fig. 1(a). The training process consists of two primary stages. First, we train the nuclei

density estimator, as shown in Fig. 1(b). In the second stage, GAN is trained with two auxiliary branches, realizing membrane staining enhancement and nuclei density regularization, as illustrated in Fig. 1(c) and Fig. 1(d), respectively.

Domain Knowledge in HER2 Scoring. In IHC-stained images, cell membranes with abnormal HER2 expression are typically stained with diaminobenzidine (DAB), appearing brown. According to HER2 guidelines [1], the clinical knowledge for HER2 scoring emphasizes the quantity of infiltrating carcinoma cells and the intensity of membrane staining (brown), where the nuclei are uniformly stained in blue. Inspired by this, in Fig. 1(a), we perform color deconvolution [19] on the real IHC-stained image to obtain the hematoxylin staining channel and the DAB staining channel $\mathcal{K}_M$ in Haematoxylin-Eosin-DAB (HED) color space. The former indicates the nuclei distribution, while the latter indicates the region of stained membranes. For the hematoxylin channel, we utilize Ostu's threshold method [16] followed by morphological operations to derive the nuclei distribution map. Based on the map, we utilize pretrained cell segmentation models to obtain the nuclei centroids. Lastly, we create a binary matrix by setting the elements corresponding to the nuclei centroids as one. This binary matrix is then transformed into a continuous density map $\mathcal{K}_N$ through convolution with a Gaussian kernel. For the DAB channel, we initially convert it into the HSV color space and subsequently derive the membrane staining intensity mask $\mathcal{M}$ by applying a threshold on the saturation channel.

Nuclei Density Estimator. The nuclei distribution offers crucial insights into the overall morphology of pathological images. Thus, we introduce an estimator E to approximate nuclei density maps, as illustrated in Fig. 1(b). E is composed of several convolution layers and residual blocks. The generator G comprises an encoder G_{en}, a decoder and several residual blocks. We leverage multiple high-level semantic features of $\mathcal{Y}$ from G_{en} to train E, with G_{en} being frozen. Subsequently, the estimator E is optimized by the loss function

$$\mathcal{L}_{estimator}(E) = \mathbb{E}_{\mathcal{Y},\mathcal{K}_N}\left[\|E((G_{en}(\mathcal{Y})), \mathcal{K}_N\|_2\right], \tag{1}$$

where $\|\cdot\|_2$ denotes the L2 distance. And $\mathcal{K}_N$ denotes true nuclei density maps generated from the knowledge extraction procedures.

Membrane Staining Enhancement. A critical aspect in HER2 scoring during routine evaluation is the assessment of membrane staining intensity [1]. Thus, a well-generated HER2-stained image should precisely depict the expression on staining membranes. To improve the preservation of staining knowledge and eliminate cellular matrix information, we introduce an auxiliary membrane staining enhancement branch for the generator. This branch operates by masking H&E-stained images with corresponding membrane staining intensity masks. The masked images are then input into the generator to produce virtual DAB channel images. Similar to the original branch, this auxiliary branch is also supervised by the pixel values of corresponding real images. However, in this case, the additional generated results are expected to approximate the DAB value distribution of real images, thereby capturing the DAB channel information, as illustrated in Fig. 1(c). Consequently, the membrane staining enhancement on

the generator is implemented by optimizing

$$\mathcal{L}_{membrane}(G) = \mathbb{E}_{\mathcal{X},\mathcal{M},\mathcal{K}_M}\left[\|G(\mathcal{M}\odot\mathcal{X}),\mathcal{K}_M\|_1\right], \tag{2}$$

where $\|\cdot\|_1$ denotes L1 distance, $\odot$ denotes pixel-wise product. G represents the generator, $\mathcal{M}$ denotes membrane staining intensity masks, and $\mathcal{K}_M$ denotes real DAB channel images.

Nuclei Density Regularization. The well-trained density estimator E is utilized to evaluate the consistency of nuclei density between real and generated IHC-stained images. When training the generator, the nuclei density estimator remains frozen. As the density estimator predicts the nuclei density maps for generated IHC-stained images, the generator is also optimized through nuclei density regularization. The corresponding loss function is formulated by

$$\mathcal{L}_{nuclei}(G) = \mathbb{E}_{\mathcal{X},\mathcal{K}_N}\left[\|E(G_{en}(G(\mathcal{X}))),\mathcal{K}_N\|_2\right], \tag{3}$$

Minimizing $\mathcal{L}_{nuclei}$ promotes the nuclei distribution alignment between the real and generated images. The method to generate nuclei density maps for generated images based on color space transformation is non-differentiable. In this case, the corresponding loss cannot be backpropagated to optimize the generator. However, the proposed density estimator overcomes this issue, enabling nuclei density regularization to guide the generator.

Training Strategy. Our objective function of GAN training is based on a conditional GAN [9], which can be expressed as

$$\mathcal{L}_{GAN}(G,D) = \mathbb{E}_{\mathcal{X},\mathcal{Y}}\left[\log D(\mathcal{X},\mathcal{Y})\right] + \mathbb{E}_{\mathcal{X}}\left[\log(1-D(\mathcal{X},G(\mathcal{X})))\right], \tag{4}$$

where G tries to minimize this objective against an adversarial D that tries to maximize it. Therefore, our final objective is

$$\begin{aligned} G^* = \arg\min_G \max_D \mathcal{L}_{GAN}(G,D) + \lambda_{L1}\mathcal{L}_{L1}(G) \\ + \lambda_N\mathcal{L}_{nuclei}(G) + \lambda_M\mathcal{L}_{membrane}(G), \end{aligned} \tag{5}$$

where λ_{L1}, λ_N, λ_M are trade-off hyper-parameters, and $\mathcal{L}_{L1}(G)$ represents the L1 loss between real and generated images.

In each iteration, we first update the nuclei density estimator by $\mathcal{L}_{estimator}$ with a coefficient λ_E. Then we update the discriminator followed by the generator, where the vanilla GAN loss is replaced with the LSGAN objective [15].

3 Experiments

Dataset. We collect RegH2I, a dataset comprising 2592 pairs of well-registered H&E-IHC images, where the IHC-stained images are processed by 4B5 antibody [10]. These slides are scanned at a magnification of 20× and cover all HER2 scores. All images are of the fixed size 1024px × 1024px and non-overlapping. We use 1992 paired images for training and 600 for testing.

Table 1. Performance comparison. The best results are highlighted in **bold**.

Experiment	Method	SSIM↑	FID↓	DISTS↓
SOTAs	CycleGAN [24]	0.3361	40.91	0.2121
	Pix2pix [9]	0.3452	47.77	0.1920
	Pix2pixHD [22]	0.3387	41.77	0.1910
	Pyramidpix2pix [13]	**0.3477**	49.32	0.1934
	ASP [11]	0.3256	64.04	0.2200
Ablation	w/o $\mathcal{L}_{nuclei}$ & $\mathcal{L}_{membrane}$	0.3423	44.01	0.1930
	w/o $\mathcal{L}_{nuclei}$	0.3448	37.77	0.1798
	w/o $\mathcal{L}_{membrane}$	0.3416	37.40	0.1830
	ours	0.3424	**33.92**	**0.1744**

Evaluation Metrics. We employ evaluation metrics from previous works, including SSIM (Structural Similarity Index Measure) and FID (Fréchet Inception Distance). As the paired images are obtained from consecutive cuts of tissues, perfect pixel-level matching is unavailable. Thus, we adopt an additional metric, DISTS (Deep Image Structure and Texture Similarity) [5], which exhibits a strong correlation with human quality judgments and demonstrates a high degree of tolerance to texture deviation.

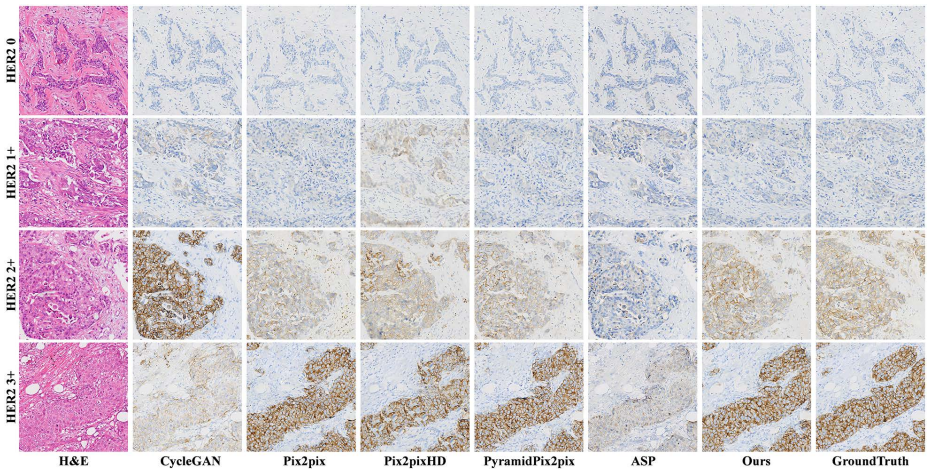

Fig. 2. Visualization of different methods on images with all HER2 scores. Note that HER2 scores here simply indicate that each image is taken from representative regions of the corresponding scored whole slide image.

Implementation Details. For the generator, we employ a 9-block ResNet [7] as the backbone. As for the discriminator, we utilize the multi-scale discriminators [22] at three image scales, with each discriminator being a 3-layer PatchGAN

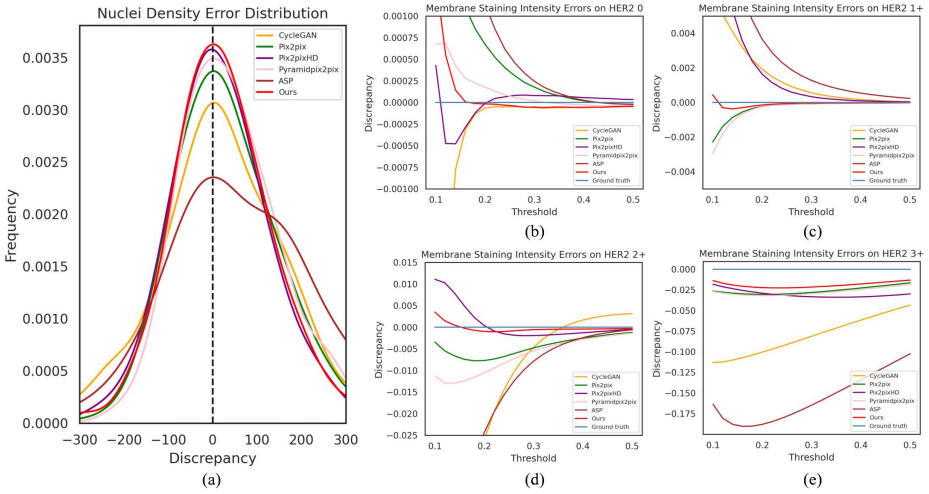

Fig. 3. The error analysis of task-specific domain knowledge. (a) Nuclei density error distribution of all methods. (b)-(e) Membrane staining intensity errors grouped by HER2 scores. The representation of HER2 scores here is the same as Fig. 2.

discriminator [9]. Regarding the density estimator, the number of residual blocks is set as 4. The utilized pretrained cell segmentation model is Cellpose [20].

Comparison with State-of-the-arts. We compare the proposed method with existing image-to-image translation and virtual staining methods, including CycleGAN [24], Pix2pix [9], Pix2pixHD [22], Pyramidpix2pix [13] and ASP [11]. The quantitative results are shown in Table 1. Generally, for metrics measuring deep feature similarity like FID and DISTS, our method achieves considerable improvements, evidenced by more convincing results in the data distribution and human perception. However, due to the inconsistency between real H&E and HER2-stained images, our proposed method achieves only moderate results compared to existing methods for the pixel-level metric SSIM. For an intuitive comparison, we show the generated images covering all HER2 scores in Fig. 2. It can be observed that our method achieves the best mapping from H&E to IHC across all HER2 expressions. This superiority is attributed to (1) unsupervised methods like CycleGAN and ASP can only achieve simple style transfer, failing to accurately detect HER2 expressions; (2) other supervised methods mainly focus on pixel alignment, lacking the preservation of key pathological information (e.g., weak staining membranes on HER2 1+ expression).

Ablation Study. We perform an ablation study to validate the effectiveness of the proposed auxiliary branches, namely membrane staining enhancement and nuclei density regularization. The corresponding results are shown in Table 1, where it can be observed that the removal of either module leads to a degradation in the performance of our method. Therefore, both the nuclei density regularization and membrane staining intensity are necessary for our method.

Table 2. HER2 staining intensity classification and H&E-to-IHC staining results on an external dataset. The best results are highlighted in **bold**. * denotes that the training and test process of classification task are both implemented on H&E images. "Real IHC images" here is only computed as a reference.

Method	Classification		Staining		
	ACC↑	F1↑	SSIM↑	FID↓	DISTS↓
H&E*	0.4246	0.3205	-	-	-
CycleGAN [24]	0.5263	0.4714	0.2915	108.74	0.2592
Pix2pix [9]	0.5930	0.5253	0.3120	128.07	0.3006
Pix2pixHD [22]	0.6386	0.5430	0.3041	104.96	0.2791
Pyramidpix2pix [13]	0.7053	0.6567	0.3071	130.08	0.2917
ASP [11]	0.5439	0.5002	0.2842	112.42	0.2510
ours	**0.7263**	**0.6795**	0.3141	104.79	0.2657
Real IHC images	0.7228	0.7298	-	-	-

Task-specific Domain Knowledge Analysis. We conduct two analyses to validate the superiority of our method in leveraging task-specific domain knowledge. For nuclei density, we calculate the difference in the number of nuclei between real and corresponding generated IHC-stained images. As shown in Fig. 3(a), our method (red line) has the maximum frequency around zero error, indicating the closest reproduction of nuclei density on generated images, attributed to the nuclei density regularization. For membrane staining intensity, we apply increasing thresholds from 0.1 to 0.5 with a step size of 0.02 to obtain a set of $\mathcal{M}$ for real and generated images. Subsequently, we calculate the ratio of $\mathcal{M}$ to the whole image for each threshold and calculate the difference between this ratio in real and generated images as the error. As depicted in Fig. 3(b)-(e), our method (red line) demonstrates more pronounced advantages as HER2 expression increases. With the auxiliary branch for membrane staining enhancement, our method achieves better consistency in membrane staining intensity.

Analysis on External Data. To further evaluate the feasibility of virtual IHC-stained images for downstream tasks, in this part, we present a dataset comprising 285 pairs of H&E-IHC images stained with SP3 [3] or CB11 [17] antibody. Specifically, we conduct a downstream classification task to distinguish four types of membrane staining intensity, in line with the guideline for HER2 scoring [1]. For each virtual staining method, we utilize the IHC-stained images (600 patches) generated previously as the training and validation set to train a ResNet50 [7] classifier, which is then evaluated on the external IHC-stained images. As shown in Table 2, the classifier trained by generated images of our method outperforms all comparative methods, even competitive with the results of the classifier trained with real IHC-stained images. Notably, the original H&E-stained images lead to poor performance for the classification task due to the disability of measuring membrane staining intensity. Therefore, accurate virtual staining from H&E to IHC on HER2 images significantly contributes to the assessment of HER2 expressions. In addition, we also present the evalua-

tion of H&E-to-IHC virtual staining in the newly presented dataset in Table 2. Since the different antibodies result in non-negligible discrepancies, substantial degradation can be observed for virtual staining. In contrast, the semantic consistency across different antibodies contributes to the transferability in classification tasks, hence, the superiority of our method validates its capability to capture diagnosis information during virtual staining.

4 Conclusions

In this paper, we propose a novel GAN model to advance H&E-to-IHC virtual staining for HER2 scoring. We introduce a nuclei density estimator to learn nuclei distribution, along with two auxiliary branches for nuclei density regularization and membrane staining enhancement, ensuring pathological consistency between real and generated images. Our method outperforms existing methods and demonstrates the importance of integrating medical insights into models for accurate virtual staining. In the future, we aim to devise a unified approach for injecting medical knowledge into models for various clinical tasks.

Acknowledgments. This work was supported by National Natural Science Foundation of China (Grant No. 62371409), the Research Grants Council of Hong Kong (T45-401/22-N and 27206123) and Hong Kong Innovation and Technology Fund (ITS/274/22).

Disclosure of Interests. The authors have no competing interests to declare that are relevant to the content of this article.

References

1. Ahn, S., Woo, J.W., Lee, K., Park, S.Y.: Her2 status in breast cancer: changes in guidelines and complicating factors for interpretation. Journal of pathology and translational medicine **54**(1), 34–44 (2020)
2. Bai, B., Yang, X., Li, Y., Zhang, Y., Pillar, N., Ozcan, A.: Deep learning-enabled virtual histological staining of biological samples. Light: Science & Applications **12**(1), 57 (2023)
3. D'Alfonso, T.M., Liu, Y.F., Chen, Z., Chen, Y.B., Cimino-Mathews, A., Shin, S.J.: Sp3, a reliable alternative to herceptest in determining her-2/neu status in breast cancer patients. Journal of clinical pathology **66**(5), 409–414 (2013)
4. De Cuyper, A., Van Den Eynde, M., Machiels, J.P.: Her2 as a predictive biomarker and treatment target in colorectal cancer. Clinical colorectal cancer **19**(2), 65–72 (2020)
5. Ding, K., Ma, K., Wang, S., Simoncelli, E.P.: Image quality assessment: Unifying structure and texture similarity. IEEE Transactions on Pattern Analysis and Machine Intelligence **44**, 2567–2581 (2020)
6. DoanNgan, B., Angus, D., Sung, L., et al.: Label-free virtual her2 immunohistochemical staining of breast tissue using deep learning. BME frontiers (2022)
7. He, K., Zhang, X., Ren, S., Sun, J.: Deep residual learning for image recognition. In: Proceedings of the IEEE conference on computer vision and pattern recognition. pp. 770–778 (2016)

8. Iqbal, N., Iqbal, N.S.: Human epidermal growth factor receptor 2 (her2) in cancers: Overexpression and therapeutic implications. Molecular Biology International **2014** (2014)
9. Isola, P., Zhu, J.Y., Zhou, T., Efros, A.A.: Image-to-image translation with conditional adversarial networks. In: Proceedings of the IEEE conference on computer vision and pattern recognition. pp. 1125–1134 (2017)
10. Karakas, C., Tyburski, H., Turner, B.M., Wang, X., Schiffhauer, L.M., Katerji, H., Hicks, D.G., Zhang, H.: Interobserver and interantibody reproducibility of her2 immunohistochemical scoring in an enriched her2-low–expressing breast cancer cohort. American Journal of Clinical Pathology **159**(5), 484–491 (2023)
11. Li, F., Hu, Z., Chen, W., Kak, A.C.: Adaptive supervised patchnce loss for learning h&e-to-ihc stain translation with inconsistent groundtruth image pairs. In: International Conference on Medical Image Computing and Computer-Assisted Intervention (2023)
12. Li, J., Luo, H., Zhu, X., Zhao, J., Chen, T.: Designing dna cage-based immunofluorescence strategy for rapid diagnosis of clinical cervical cancer tissues. Chinese Chemical Letters **33**(2), 788–792 (2022)
13. Liu, S., Zhu, C., Xu, F., Jia, X., Shi, Z., Jin, M.: Bci: Breast cancer immunohistochemical image generation through pyramid pix2pix. 2022 IEEE/CVF Conference on Computer Vision and Pattern Recognition Workshops (CVPRW) pp. 1814–1823 (2022)
14. Liu, S., Zhang, B., Liu, Y., Han, A., Shi, H., Guan, T., He, Y.: Unpaired stain transfer using pathology-consistent constrained generative adversarial networks. IEEE Transactions on Medical Imaging **40**, 1977–1989 (2021)
15. Mao, X., Li, Q., Xie, H., Lau, R.Y.K., Wang, Z., Smolley, S.P.: Least squares generative adversarial networks. 2017 IEEE International Conference on Computer Vision (ICCV) pp. 2813–2821 (2016)
16. Otsu, N.: A threshold selection method from gray-level histograms. IEEE Trans. Syst. Man Cybern. **9**, 62–66 (1979)
17. Purdie, C.A., Jordan, L.B., McCullough, J.B., Edwards, S.L., Cunningham, J., Walsh, M., Grant, A., Pratt, N., Thompson, A.M.: Her2 assessment on core biopsy specimens using monoclonal antibody cb11 accurately determines her2 status in breast carcinoma. Histopathology **56**(6), 702–707 (2010)
18. Rivenson, Y., de Haan, K., Wallace, W.D., Ozcan, A.: Emerging advances to transform histopathology using virtual staining. BME frontiers **2020** (2020)
19. Ruifrok, A.C., Johnston, D.A.: Quantification of histochemical staining by color deconvolution. Analytical and quantitative cytology and histology **23 4**, 291–9 (2001)
20. Stringer, C., Wang, T., Michaelos, M., Pachitariu, M.: Cellpose: a generalist algorithm for cellular segmentation. Nature Methods **18**, 100 – 106 (2020)
21. Swain, S.M., Shastry, M., Hamilton, E.: Targeting her2-positive breast cancer: Advances and future directions. Nature Reviews Drug Discovery **22**(2), 101–126 (2023)
22. Wang, T.C., Liu, M.Y., Zhu, J.Y., Tao, A., Kautz, J., Catanzaro, B.: High-resolution image synthesis and semantic manipulation with conditional gans. 2018 IEEE/CVF Conference on Computer Vision and Pattern Recognition pp. 8798–8807 (2017)
23. Zeng, B., Lin, Y., Wang, Y., Chen, Y., Dong, J., Li, X., Zhang, Y.: Semi-supervised pr virtual staining for breast histopathological images. In: International Conference on Medical Image Computing and Computer-Assisted Intervention (2022)

24. Zhu, J.Y., Park, T., Isola, P., Efros, A.A.: Unpaired image-to-image translation using cycle-consistent adversarial networks. 2017 IEEE International Conference on Computer Vision (ICCV) pp. 2242–2251 (2017)